Chemical Physics Letters 499 (2010) 136–140

Contents lists available at ScienceDirect

Chemical Physics Letters

journal homepage: www.elsevier.com/locate/cplett

The interfacial electronic structure of fullerene/ultra thin dielectrics of SiO_2 and SiON

S.W. Cho [a], Y. Yi [b,*], K.B. Chung [c], S.J. Kang [d], M.-H. Cho [e,**]

[a] Department of Physics, Boston University, 590 Commonwealth Ave., Boston, MA 02215, USA
[b] Division of Industrial Metrology, Korea Research Institute of Standards and Science, 209 Gajeong-Ro, Yuseong-Gu, Daejeon 305-340, Republic of Korea
[c] Department of Physics, Dankook University, Dongnamgu, Anseodong 29, Cheonan 330-714, Republic of Korea
[d] Department of Advanced Materials Engineering for Information and Electronics, Kyung Hee University, Seocheon-dong, Giheung-gu, Yongin 446-701, Republic of Korea
[e] Institute of Physics and Applied Physics, Yonsei University, 134 Shinchon-dong, Seodaemoon-gu, Seoul 120-749, Republic of Korea

ARTICLE INFO

Article history:
Received 7 July 2010
In final form 7 September 2010
Available online 15 September 2010

ABSTRACT

The electronic structures at the interface region between fullerene and dielectric layers were investigated by *in situ* ultraviolet photoelectron spectroscopy (UPS) and X-ray photoelectron spectroscopy (XPS). The highest occupied molecular orbital (HOMO) onset of the fullerene layer saturates at 1.3 eV below the Fermi level of the SiO_2 layer, which was based on the measurement of the sample with a 12.8 nm thick fullerene layer. On the other hand, the HOMO onset was measured at 2.0 eV below the SiON layer Fermi level. The magnitude of the interface dipole and band bending at the interface was determined, and the complete energy level diagrams for fullerene on SiO_2 and SiON were evaluated.

© 2010 Elsevier B.V. All rights reserved.

1. Introduction

Organic electronics are expending their areas of application and showing significant advances in device performance. Among organic devices, organic thin-film transistors (OTFTs) have been eagerly researched because of their many applications, such as flexible displays, pliable electronic paper, radio-frequency identification tags, and smart cards [1–7]. Certainly organic films have several advantages over inorganic semiconductors, although the former have poorer electrical properties than the latter; the operating voltage required for OTFTs is too high for practical use. Accordingly, development of low-voltage operating OTFTs has become a priority. Recently, low-voltage driven OTFTs that use high-*k* metal oxides [8,9], organic gate dielectrics [10,11], and double gate dielectric layers [12,13] have been reported. The control of the threshold voltage during low-voltage operation depends not only on the gate dielectric constants, but also on the interfacial electronic structures between the dielectric layers and the organic semiconductors [14]. Therefore, understanding of interfacial electronic structures is becoming more and more important. In this study, the electronic structures at the interface between fullerene (C_{60}), which is a prototype active layer for *n*-type OTFTs, and ultra thin (4.5 nm) dielectric layers of SiO_2 and SiON were studied. SiO_2 is used widely as a gate dielectric in commercial thin-film transistors. With extensive knowledge of the behavior of such devices, SiO_2 is also commonly used as a dielectric for OTFTs. However, attempts to reduce the thickness of SiO_2 to less than 2 nm for low-voltage operating have clearly demonstrated the limitations of SiO_2: high leakage current and poor resistance to boron penetration. Therefore, nitrided silicon oxide (SiON) has replaced the conventional SiO_2 in dielectric applications. To understand the performance of these devices, we compared the interfacial electronic structures of C_{60}/SiO_2 and C_{60}/SiON. Chemical reactions and band bending at the interface were investigated using X-ray photoelectron spectroscopy (XPS). The shifts in vacuum level and in the highest occupied molecular orbital (HOMO) level were examined through ultraviolet photoelectron spectroscopy (UPS). The electronic structure of the organic/metal [15], organic/insulator [16], and organic/organic interfaces [17] has been studied by several research groups. In this study, detailed electronic structures of the C_{60}/SiO_2 and C_{60}/SiON systems and complete energy level diagrams are described.

2. Experimental

The 4.5 nm SiO_2 layers were grown at 400 °C using a plasma oxidation process on *p*-type Si(0 0 1) wafers cleaned by the standard Radio Corporation of America method [18]. A mixture of Ar/O_2 gas as a medium for plasma was introduced through the discharge cavity under a microwave power of 100 W. The film layer showed superior gate dielectric properties such as a reduced transition layer and high charge-to-breakdown to thermally grown SiO_2 [19]. The nitridation process was performed using a RF source

* Corresponding author. Fax: +82 42 868 5032.
** Corresponding author.
E-mail addresses: yeonjin@kriss.re.kr (Y. Yi), mh.cho@yonsei.ac.kr (M.-H. Cho).

0009-2614/$ - see front matter © 2010 Elsevier B.V. All rights reserved.
doi:10.1016/j.cplett.2010.09.024

(inductively coupled plasma, 13.56 MHz) at an rf power of 700 W and the substrate temperature of 400 °C. The N_2 flow rate was set by a mass flow controller at 60 sccm and the process pressure was fixed at 500 mTorr [20]. The thickness and chemical composition of each dielectric layer were determined using medium-energy ion scattering (MEIS) spectroscopy.

To investigate the interface formation and the resulting electronic structures, C_{60} was evaporated in a stepwise manner on sputter-cleaned SiO_2 and SiON substrates at room temperature. The deposition rate of C_{60} was kept at 0.1 Å/s and the accumulated layer thickness was monitored using a calibrated quartz thickness monitor. The background pressure of the preparation chamber was maintained at 1.4×10^{-9} Torr during film deposition. The valence band (sample bias: −15 V) and core-level spectra were collected without breaking the vacuum after each deposition step was completed. The XPS and UPS spectra were obtained on a PHI 5700 spectrometer using standard Al Kα (1486.6 eV) and He I (21.2 eV) sources. The base pressure of the analysis chamber was 2×10^{-10} Torr.

3. Results and discussion

Figure 1 illustrates the procedure used for the determination of energy level alignment at the interface. The basic equation used in interpreting photoelectron spectra is:

$$E_B = h\nu - E_k - \Phi \quad (1)$$

The photon energy ($h\nu$) is known and the photoelectron kinetic energy (E_k) is measured in order to deduce the binding-energy (E_B) referenced to the Fermi level (E_F). When $h\nu$ is known, the work function (Φ) can be obtained from the measured energy of the secondary electron cut-off ($E_{cut\text{-}off}$), i.e.:

$$\Phi = h\nu - E_{cut\text{-}off} \quad (2)$$

The change in the work function, $\Delta\Phi$, can then be tracked by measuring $E_{cut\text{-}off}$ after a deposition step. Therefore, the shift of this $E_{cut\text{-}off}$ indicates the magnitude of the interfacial dipole, which is equal to increases or decreases the work function [21,22]. Similarly, the ionization energy (IE) can be obtained from $E_{cut\text{-}off}$ and the HOMO onset (E_{HOMO}):

$$IE = h\nu - (E_{cut\text{-}off} - E_{HOMO}) \quad (3)$$

The electronic structure at the interface between the C_{60} and dielectric layers was investigated using *in situ* UPS and XPS. Figures 2 and 3 show the UPS spectra during the deposition of C_{60} on SiO_2 and SiON. The spectra shown in Figure 2a and b were collected in the secondary electron cut-off region for the SiO_2 and SiON layers, respectively. The secondary cut-off position moved noticeably towards lower binding-energy as soon as the C_{60} deposition began on each substrate. The shift of the secondary cut-off position is attributed to the formation of an interface dipole [21] and/or band bending. The total shift of the cut-off position was 0.2 eV for the SiO_2 and 0.3 eV for the SiON layer.

Figure 3a and b shows the evolution of HOMO onset during the growth of the C_{60} layer on SiO_2 and SiON, respectively. When the coverage of C_{60} was greater than 0.4 nm, the features attributable to the C_{60} layer were dominant. In addition, the HOMO of C_{60} gradually shifted towards lower binding energies for both interfaces. These shifts correspond to the band bending at the interfaces. The magnitudes of band bending in the UPS spectra were 0.2 eV for the SiO_2 and 0.3 eV for the SiON, which we could confirm from the C 1*s* core-level spectra. The shift in the HOMO onset was saturated as the thickness of the C_{60} layer increased. The saturated HOMO onset of the C_{60} layer was 1.3 eV below the Fermi level for the SiO_2 layer, based on the spectrum with a 12.8 nm thick C_{60} layer. The saturated HOMO onset was measured at 2.0 eV for the SiON layer. No additional shift in the onset position was observed for either the SiO_2 or the SiON layer when the thickness of the C_{60} layer was greater than 12.8 nm, indicating that the interaction between C_{60} and the dielectric layer was confined to a short range and that no further interactions occurred as the C_{60} layer thickened.

The core-level spectra of the sample were also collected during the step-by-step deposition to investigate the band bending and chemical reaction between the layers. Figure 4 shows the core-level spectra of C 1*s*, obtained during C_{60} deposition on SiO_2 and SiON. The line shapes of these spectra were analyzed using a

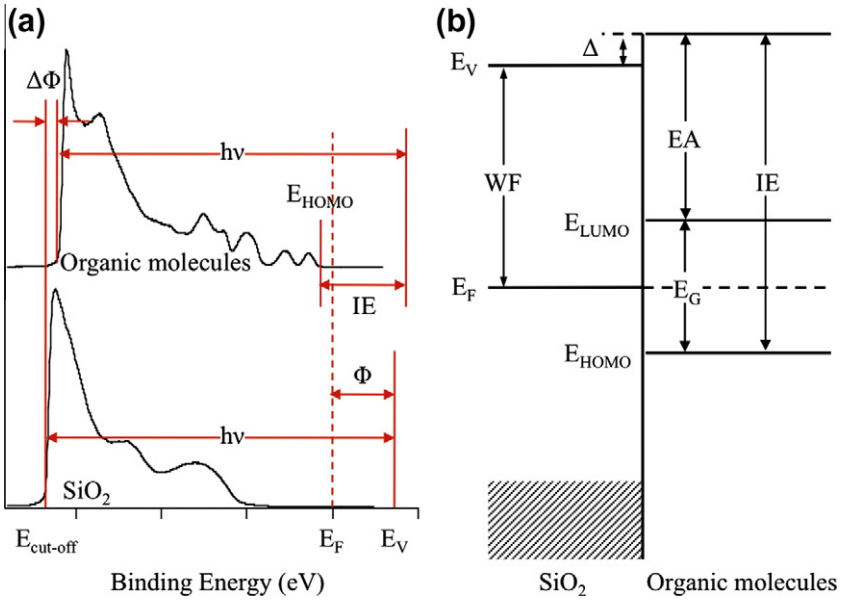

Figure 1. (a) Schematic illustration of the important parameters derived from PES characterization of surfaces and interfaces. (b) A band diagram for a generic junction formed between an organic film and a dielectric substrate.

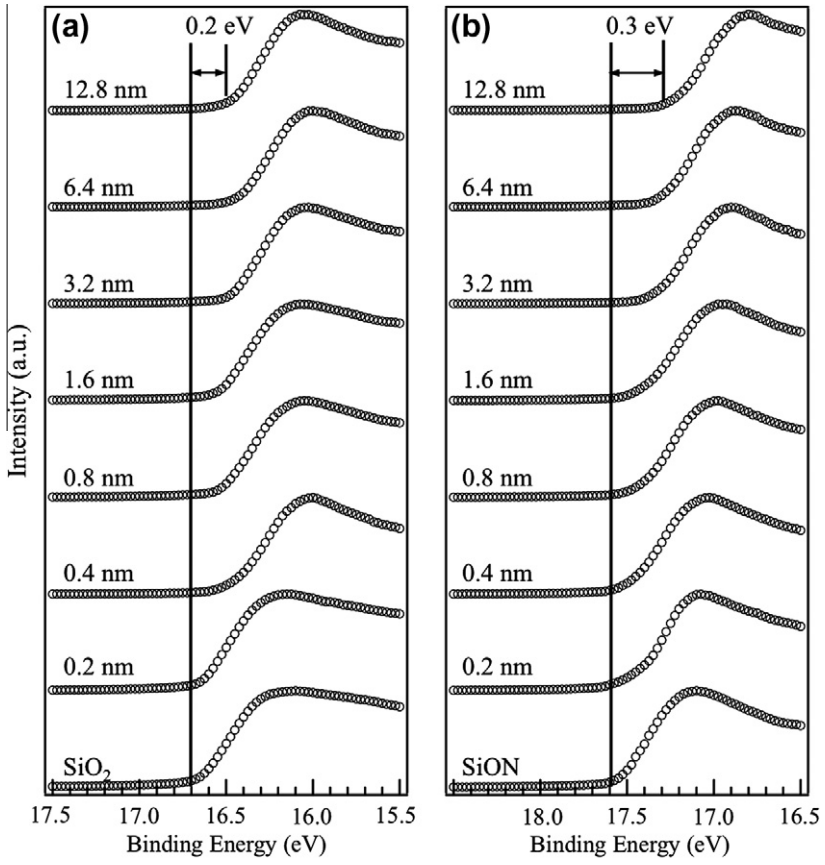

Figure 2. The UPS spectra in the secondary electron cut-off region collected during the step-by-step layer deposition of C_{60} on (a) the SiO_2 surface and on (b) the SiON surface.

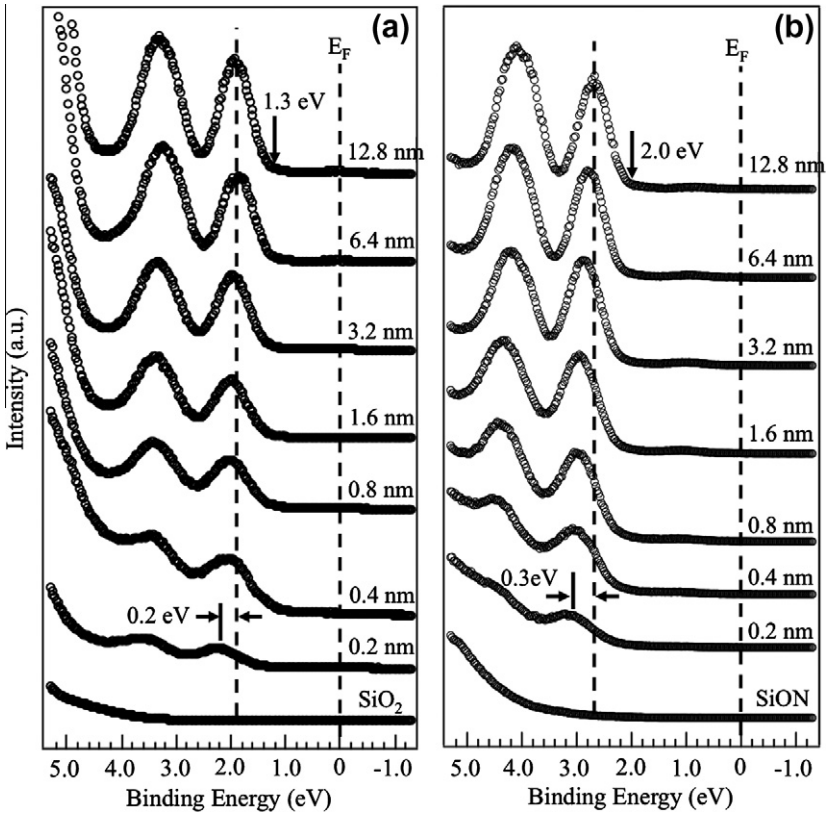

Figure 3. The UPS spectra collected near the Fermi level as a function of C_{60} deposition thickness on (a) the SiO_2 surface and on (b) the SiON surface.

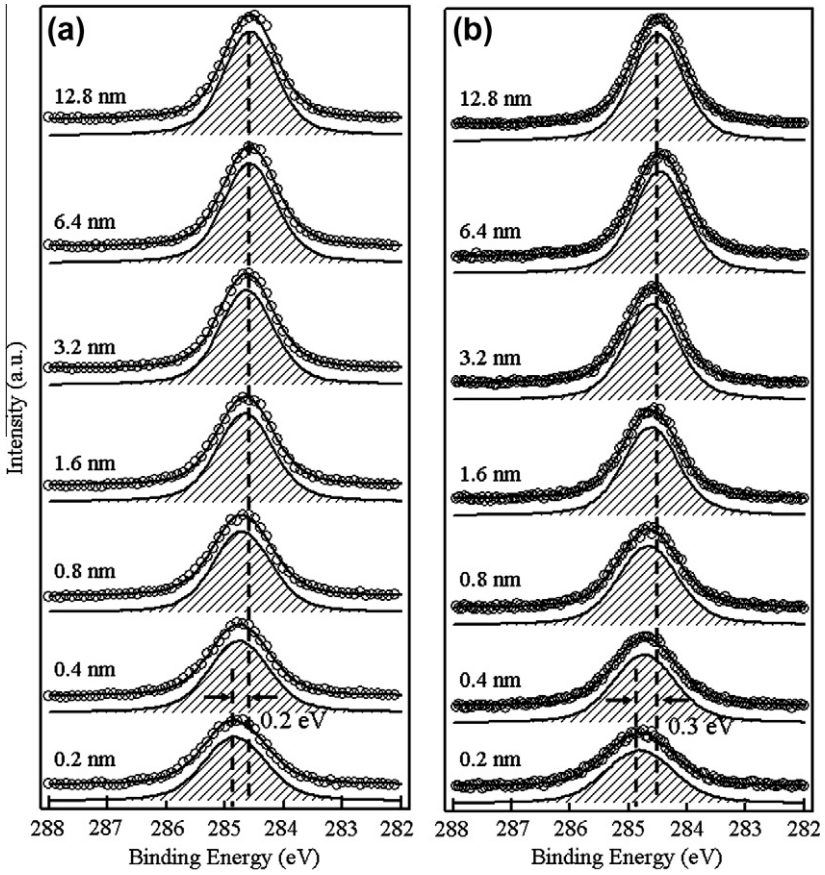

Figure 4. The core-level spectra of C 1*s* obtained during the C_{60} deposition on (a) the SiO_2 surface and on (b) the SiON surface, respectively.

standard least-squares fitting scheme. Figure 4a shows only one C 1*s* component for pristine C_{60} and it means no reaction between C_{60} and the SiO_2 substrate. A noticeable shift of the C 1*s* core-level peak towards lower binding energies was observed as the thickness of the C_{60} layer increased. The total C 1*s* peak shift was 0.2 eV, which matches quite well with the shift of HOMO on the SiO_2 layer. These findings also confirm the band bending of 0.2 eV at the C_{60}/SiO_2 interface [23]. The energy level gradually reached its intrinsic position as a function of the C_{60} thickness. The C 1*s* spectra in Figure 4b obtained during C_{60} deposition on SiON also reveal no reaction between C_{60} and the SiON substrate. The total C 1*s* peak shift was 0.3 eV, consistent with the shift of HOMO for the SiON layer (Figure 3b). Although secondary cut-off shifts were observed, they do not correspond to interface dipoles at either interface after subtracting the contributions of band bending. The change in secondary electron cut-off, i.e. work function, contains both contributions of the band bending and the interface dipole [24]. Therefore, the interface dipole at the interface should be evaluated after subtracting band bending from the total secondary cut-off change (or work function change). In this case, the amount of secondary cut-off shift (0.3 eV) is the same as that of band bending, thus there is negligible interface dipole.

An energy level diagram was constructed by combining the changes in spectra shown in Figures 2–4. As shown in Figure 5, the energy gap between HOMO and LUMO was about 2.6 eV, as previously reported [25]. Generally, in an energy diagram, when a positive gate voltage is applied for the operation of the C_{60} TFTs, the gate voltage bends the LUMO levels down towards the Fermi level. Then, mobile electron carriers accumulate and form a conducting channel. These band diagrams show that a lower voltage is needed to bend the LUMO level towards the Fermi level in the

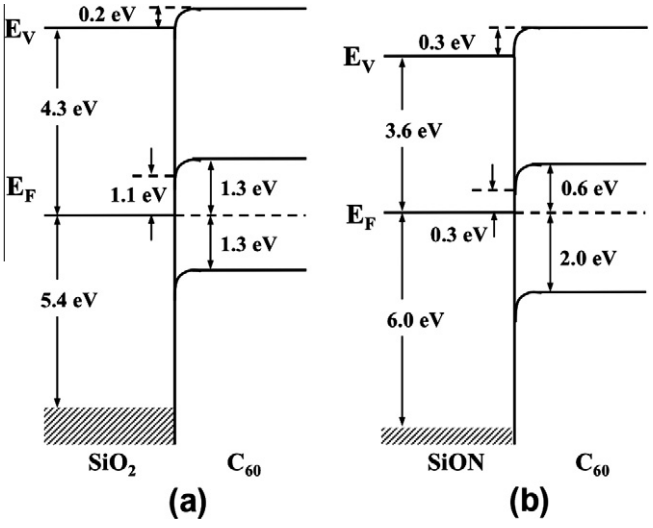

Figure 5. Energy level diagrams of C_{60} on (a) the SiO_2 surface and on (b) the SiON surface.

C_{60}/SiON layer as compared to the C_{60}/SiO_2 layer because the Fermi level is closer to the LUMO level at the C_{60}/SiON interface than to at the C_{60}/SiO_2 interface [26]. Thus, it follows that the OTFTs with SiON gate dielectric layers might have lower operating gate voltages and lower threshold voltages than those of the SiO_2 OTFTs. According to the traditional Schottky–Mott model, the LUMO offset is simply the difference between the electron affinity of C_{60} and the work function of the substrate. In reality, interface dipoles and

band bending should be considered to predict the exact LUMO offset. In this study, the measured work functions of SiO_2 and SiON are estimated to be about 4.3 and 3.6 eV, respectively. Not only the work function but also the IE of ~9.7 eV for the SiO_2 surface agrees reasonably well with the values expected from the band gap (~9 eV) and electron affinity (~1.0 eV) [27–29]. As mentioned above, there is no interface dipole on either the C_{60}/SiO_2 or C_{60}/SiON interface. This reflects the lack of chemical interaction and the minimal electronic interaction at these interfaces. Although each interface of C_{60}/SiO_2 and C_{60}/SiON has a different amount of band bending, which would affect the interfacial LUMO position of C_{60}, we find that this difference (0.1 eV) is much smaller compared to the work functions difference (0.7 eV) between two dielectrics. Thus, the LUMO offset with respect to the Fermi level is determined mainly by the initial work function of each dielectric substrate. This matches well with the dipole free interface on both substrates, which follows the traditional Schottky–Mott limit [30] (slope parameter ≈ 1). Fukagawa et al. has reported that for substrate work functions smaller than the IE of pentacene, slope parameter = 1, whereas for substrate work functions exceeding the IE, the formation of an interface dipole is clearly displayed [31]. The work functions of SiO_2 and SiON are also smaller than the IE of C_{60} (5.8–5.9 eV). Therefore, it confirms that the operating gate voltage of *n*-type OTFTs using C_{60} is mainly related to the work function of the specific dielectric layer used. If the other properties were similar, the dielectric layer with a low work function would be better for a low-voltage operating *n*-type OTFTs using C_{60}. It has been reported that the work function can be tuned by adjusting the nitrogen compositions and the high nitrogen content results in reducing the work function of the films [32]. As reported MEIS spectra of SiON film, the nitrogen content was effectively localized on the surface of the film [20]. This surface nitrogen reduces the work function of the SiON layer because the nitrogen attracts electrons less strongly than the oxygen.

4. Conclusions

The electronic structures at the interface region between C_{60} and the dielectric layers for the lower operating voltage were investigated by *in situ* UPS and XPS. The saturated HOMO onset of the C_{60} layer was 1.3 eV below the Fermi level for the SiO_2 layer, which was based on the measurement of the sample with a 12.8 nm thick C_{60} layer. The HOMO onset was measured at 2.0 eV for the SiON layer. The magnitude of the interface dipole and band bending at the interface were determined, and the complete energy level diagrams for C_{60} on SiO_2 and SiON were evaluated. The results confirm that the shift of the threshold voltage and the turn-on voltage is related to the work function of the specific dielectric layer used.

Acknowledgements

This work was supported by Korea Research Council of Fundamental Science and Technology (KRCF) through the KRISS project of 'Development of Advanced Industrial Metrology', a research project of the Korea Research Foundation (Grant No. 2009-0070876), and New and Renewable Energy R&D program (Grant No. 2009T100100614) under the Ministry of Knowledge Economy, Republic of Korea.

References

[1] C.D. Dimitrakopoulos, P.R.L. Malenfant, Adv. Mater. 14 (2) (2002) 99.
[2] H.E.A. Huitema, G.H. Gelinck, J.B.P.H. van der Putten, K.E. Kuijk, K.M. Hart, E. Cantatore, D.M. de Leeuw, Adv. Mater. 14 (17) (2002) 1201.
[3] B. Comiskey, J.D. Albert, H. Yoshizawa, J. Jacobson, Nature 394 (6690) (1998) 253.
[4] C.D. Sheraw et al., Appl. Phys. Lett. 80 (6) (2002) 1088.
[5] F. Eder, H. Klauk, M. Halik, U. Zschieschang, G. Schmid, C. Dehm, Appl. Phys. Lett. 84 (14) (2004) 2673.
[6] R. Wisnieff, Nature 394 (6690) (1998) 225.
[7] P.F. Baude, D.A. Ender, M.A. Haase, T.W. Kelley, D.V. Muyres, S.D. Theiss, Appl. Phys. Lett. 82 (22) (2003) 3964.
[8] Y. Liang, G.F. Dong, Y. Hu, L.D. Wang, Y. Qiu, Appl. Phys. Lett. 86 (13) (2005) 132101.
[9] L.A. Majewski, R. Schroeder, M. Grell, Adv. Mater. 17 (2) (2005) 192.
[10] L.L. Chua, P.K.H. Ho, H. Sirringhaus, R.H. Friend, Appl. Phys. Lett. 84 (17) (2004) 3400.
[11] M.H. Yoon, H. Yan, A. Facchetti, T.J. Marks, J. Am. Chem. Soc. 127 (29) (2005) 10388.
[12] D.K. Hwang et al., Adv. Mater. 18 (17) (2006) 2299.
[13] D.K. Hwang et al., Appl. Phys. Lett. 88 (24) (2006) 243513.
[14] S.W. Cho, J.G. Jeong, S.H. Park, M.H. Cho, K. Jeong, C.N. Whang, Y. Yi, Appl. Phys. Lett. 92 (21) (2008).
[15] I.G. Hill, A. Rajagopal, A. Kahn, J. Appl. Phys. 84 (6) (1998) 3236.
[16] N.J. Watkins, S. Zorba, Y.L. Gao, J. Appl. Phys. 96 (1) (2004) 425.
[17] H. Ishii, K. Sugiyama, E. Ito, K. Seki, Adv. Mater. 11 (8) (1999) 605.
[18] W. Kern, Handbook of Semiconductor Wafer Cleaning Technology: Science, Technology, and Applications, William Andrew Publishing/Noyes, Park Ridge, NJ, 1993.
[19] S. Hyun et al., Appl. Phys. Lett. 85 (6) (2004) 988.
[20] M.H. Cho et al., Electrochem. Solid State 9 (5) (2006) F27.
[21] S.T. Lee, X.Y. Hou, M.G. Mason, C.W. Tang, Appl. Phys. Lett. 72 (13) (1998) 1593.
[22] C. Shen, A. Kahn, Org. Electron. 2 (2) (2001) 89.
[23] R. Schlaf, B.A. Parkinson, P.A. Lee, K.W. Nebesny, N.R. Armstrong, J. Phys. Chem. 103 (1999) 2984.
[24] H. Lüth, Solid Surfaces, Interfaces, and Thin Films, fourth Edn., Springer, New York, 2001.
[25] R. Mitsumoto et al., J. Electron Spectrosc. Relat. Phenom. 78 (1996) 453.
[26] K.P. Pernstich et al., J. Appl. Phys. 96 (11) (2004) 6431.
[27] S.M. Sze, Physics of Semiconductor Devices, Wiley, New York, 1981.
[28] E.A. Silinsh, V. Capek, Interaction, Localization, and Transport Phenomena, American Institute of Physics, New York, 1994.
[29] N.J. Watkins, Y. Gao, J. Appl. Phys. 94 (9) (2003) 5782.
[30] I.G. Hill, A. Rajagopal, A. Kahn, Y. Hu, Appl. Phys. Lett. 73 (5) (1998) 662.
[31] H. Fukagawa, S. Kera, T. Kataoka, S. Hosoumi, Y. Watanabe, K. Kudo, N. Ueno, Adv. Mater. 19 (5) (2007) 665.
[32] P.H. Tsai, K.S. Chang-Liao, T.C. Wang, T.K. Wang, C.H. Tsai, C.L. Cheng, Appl. Phys. Lett. 90 (13) (2007).